Journal of Anatomy

J. Anat. (2014) **225**, pp519–526 doi: 10.1111/joa.12230

Depth-dependent shear behavior of bovine articular cartilage: relationship to structure

Mostafa Motavalli,[1] Ozan Akkus[1,2,3] and Joseph M. Mansour[1,3]

[1]*Department of Mechanical and Aerospace Engineering, Case Western Reserve University, Cleveland, OH, USA*
[2]*Department of Biomedical Engineering, Case Western Reserve University, Cleveland, OH, USA*
[3]*Department of Orthopaedics, Case Western Reserve University, Cleveland, OH, USA*

Abstract

The mechanical behavior of bovine articular cartilage in shear was measured and related to its structure through the depth of the tissue. To make these measurements, we designed an apparatus that could apply controlled shear displacement and measure the resulting shear force on cartilage specimens. Shear displacement and shear strain were obtained from confocal images of photobleached lines on fluorescently stained deformed samples. Depth-dependent collagen structure was obtained using compensated polarized light microscopy. Depth-dependent shear behavior and structure of samples from two animals were measured (group A and B). Both animals were 18–24 months old, which is the range in which they are expected reach skeletal maturity. In mature samples (group A), the stiffest region was located beneath the superficial zone, and the most compliant region was found in the radial zone. In contrast, in samples that were in the process of maturing (group B) the most compliant region was located in the superficial zone. Compensated polarized light microscopy suggested that the animal from which the group A samples were obtained was skeletally mature, whereas the animal yielding the group B samples was in the process of maturing. Compensated polarized light microscopy was an important adjunct to the mechanical shear behavior in that it provided a means to reconcile differences in observed shear behavior in mature and immature cartilage. Although samples were harvested from two animals, there were clear differences in structure and shear mechanical behavior. Differences in the depth-dependent shear strain were consistent with previous studies on mature and immature samples and, based on the structural variation between mature and immature articular cartilage, their mechanical behavior differences can be tenable. These results suggest that age, as well as species and anatomic location, need to be considered when reporting mechanical behavior results.

Key words: articular cartilage; collagen structure; compensated polarized light microscopy; depth dependence; maturity; simple shear.

Introduction

Articular cartilage is a hypocellular, avascular, hydrated and dense soft connective tissue which provides a low-friction, wear-resistant bearing surface in diarthrodial joints and distributes stresses to underlying bone. The outward appearance of cartilage as a simple thin layer covering the articulating joint surfaces disguises its complex internal structure, and unique functional and mechanical properties.

According to previous studies (Neu et al. 2005; Buckley et al. 2008, 2010, 2013; Canal et al. 2008), structural, regional and interspecies differences (Athanasiou et al. 1991; Hunziker et al. 2002, 2007; Canal et al. 2008) give rise to varying mechanical behavior. For example, type II collagen in adult articular cartilage is oriented parallel to the articular surface in the superficial zone, but perpendicular to the subchondral bone in the radial and calcified zones. Unlike mature mammalian articular cartilage, immature cartilage is more isotropic in structure at birth and during postnatal growth (Hunziker et al. 2002, 2007). Such structural differences may give rise to different depth-dependent mechanical behavior.

Although several essentially standardized mechanical tests have been used to derive the average mechanical properties of full thickness tissue, the growing appreciation of the importance of depth-dependent properties has led to the development of new methods for mechanical evaluation (Guilak, 1995; Buckley et al. 2008, 2010; Hosoda et al. 2008; Wong & Sah, 2010). Depth-dependent behavior is

Correspondence
Mostafa Motavalli, Department of Mechanical and Aerospace Engineering, Case Western Reserve University, 616A Glennan Building, 2123 Martin Luther King Jr. Drive, Cleveland, OH 44106-7222, USA. E: sxm591@case.edu

Accepted for publication *24 July 2014*
Article published online *21 August 2014*

often evaluated using methods based on optical imaging as pioneered by Schinagl et al. (1996). In this study, we designed an apparatus to measure continuous spatial variations of the shear properties of soft tissue and implemented previously developed imaging techniques for determining the depth-dependent shear deflection of articular cartilage (Bruehlmann et al. 2004; Buckley et al. 2010; Motavalli et al. 2013). To simulate the continuous depth–dependent deflection using pixel-size data, we applied a previously developed and validated image–processing technique (Motavalli et al. 2013).

The purpose of this investigation was to determine depth-dependent shear behavior of articular cartilage and relate this to structural organization. We focused on bovine cartilage from animals that were 18–24 months old, as this is the age range in which they reach skeletal maturity and we therefore are likely to find differences in structure between animals (Kim et al. 1995; Hunziker et al. 2002, 2007; Kilborn et al. 2002).

Methods

Depth-dependent shear properties of cartilage were determined using an approach pioneered by Bruehlmann et al. (2004) for intervertebral disc and developed for articular cartilage by Buckley et al. (2010). Shear displacement was applied to a fluorescently labeled sample (Motavalli et al. 2013) and the corresponding displacement field through the thickness of the sample was obtained from confocal microscope images of deformed photobleached lines (FluoView FV1000 with 10×, 0.3 NA water immersion objective, UMPLFLN 10XW; Olympus, Center Valley, PA, USA). Displacement was applied using a two-dimensional linear stage with angular deviation < 100 μrad under rated load about any axis (ULTRAlign 461-X-M; Newport Corp., Irvine, CA, USA). Samples were attached to polymethylmethacrylate (PMMA) surfaces rather than directly to the faces of the stainless steel arms (Fig. 1) using cyanoacrylate-based ISO-10993 Biological Tested Instant Adhesive (4011; Loctite Corp., Rocky Hill, CT, USA). Samples were fluorescently labeled by immersing them in a saturated solution of dichlorotriazinylaminofluorescein (5-DTAF; Invitrogen, Grand Island, NY, USA) in phosphate-buffered saline (PBS) for about 20 min. Forces on the sample were measured using a multi-axial load cell that was sampled at 100 Hz (Nano 17; ATI Industrial Automation, Apex, NC, USA) (Fig. 1).

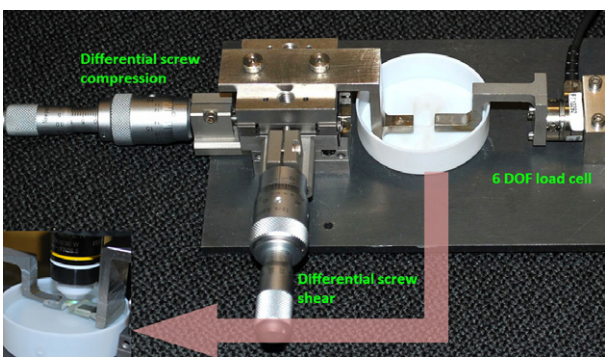

Fig. 1 Apparatus designed to apply shear and compressive displacements on a sample using differential screws. A six degree-of-freedom load cell measures the resulting shear and compressive forces. This apparatus is secured to the stage of a confocal microscope. A water immersion objective lens is used since the sample is immersed in PBS. The inset shows the sample on the stage of the upright confocal microscope, sandwiched between the PMMA caps, which were bonded to stainless steel arms. Measurements were made near the center of the sample as measured parallel to the face of the PMMA caps.

Sample preparation

Samples were harvested from the patellofemoral groove of two 18–24-month-old steers (Halal Meat, Cleveland, OH, USA). Initially, 2-cm osteochondral cubes were harvested from each joint and frozen on the same day of slaughtering. Samples were grouped according the animal they were taken from as either group A ($n = 4$) or group B ($n = 4$). On the day of testing, a full thickness rectangular (~6 × 4 mm) cartilage explant was harvested from a once-frozen osteochondral cube sample, and thawed in PBS. Isolated samples were cut and tested in the same direction that patella slides in the groove.

Mechanical testing

A construct consisting of the PMMA caps and cartilage sample was glued to the arms of the testing device and immersed in PBS to maintain hydration during the test. Using the differential micrometer (DM-13; Newport Corp.) on the linear stage, incremental shear deflections of 100 μm were applied to a sample, which results in shear strain increments of ~10% depending on sample thickness. Following each step, shear force was allowed to relax before an image was taken.

The testing device and sample were placed on the stage of an upright confocal microscope. Three parallel lines, near the center of the sample, approximately 50–70 μm apart, were photobleached across the thickness of the sample. This region was chosen because finite element analysis demonstrated uniform shear stresses within this region (Chung et al. 2012).

Imaging acquisition and analysis

Lines were photobleached using a 405-nm wavelength laser at full power. For imaging, samples were rastered using a 488-nm laser, about 50–70 μm below the surface, with 30% power, providing images of uniform brightness.

Shear strain was determined from the slope of the photobleached lines on sheared samples (Fig. 2). A custom MATLAB script was used to locate the lowest intensity pixel in each line and at each pixel through the thickness of a sample (Motavalli et al. 2013). These were averaged at each depth to produce a single sequence of values for the depth-dependent shear deflection. Depth-dependent shear strain was then found using a previously developed image processing method that employs pixel-size data to find a continuous polynomial shear displacement function fit to the deflected line (Fig. 2A1,B1) (Motavalli et al. 2013). Although the displacement of the linear stage was known, actual total shear displacement on the sample was computed from deformed images.

Shear stress (τ) was calculated using shear force, which was assumed to be constant through the thickness and area of each sample. Shear modulus was calculated at each pixel through the depth of the sample using:

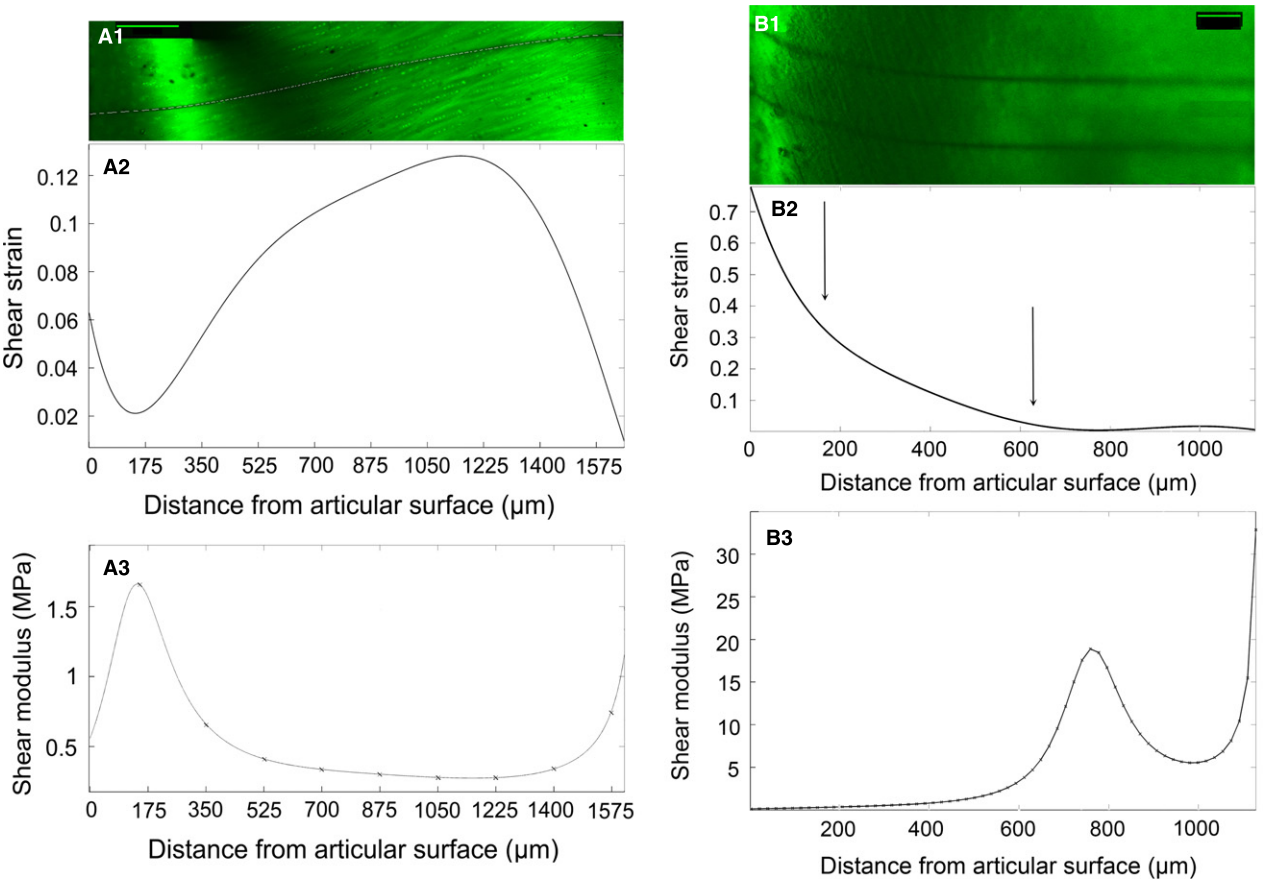

Fig. 2 (A1) Deformed photobleached line overlaid with the fitted curve used to predict the depth-dependent shear deflection and shear strain (group A) (Motavalli et al. 2013). Articular surface is at the left side of the image. Scale bar: 200 μm. (A2) Shear strain profile through the full thickness of a cartilage sample from group A, computed from the shown fitted curve. The least strain was found below the articular surface while the highest was in the radial zone. The average shear strain is 8%. (A3) Full thickness shear modulus at 8% shear strain. The stiffest region is below the articular surface, whereas the radial zone is relatively compliant for all group A samples. All group A samples demonstrated the same depth-dependent behavior. (B1) Deformed photobleached lines in group B samples. Articular surface is at the left side of the image. Scale bar: 100 μm. (B2) Shear strain profile through the full thickness of a cartilage sample from group B. The most compliant region was found on the articular surface. Break points on the depth-dependent shear strain were observed on the borders of this layer. The average shear strain is about 10%. (B3) Full thickness shear modulus at 10% shear strain. The most compliant region is below the articular surface, whereas the radial zone is relatively stiff for all group B samples. All group B samples demonstrated the same depth-dependent behavior.

$$G_d = \frac{\tau}{\gamma_d}$$

where γ_d is depth-dependent shear strain profile. The mean shear modulus was also computed using total shear strain and shear forces to evaluate shear stiffening behavior.

A randomized block ANOVA test was employed to evaluate the significance of changes in shear modulus as function of strain. A pairwise Tukey test was used to determine which strain levels differed. In this test, adjusted *P*-values < 0.05 are considered statistically significant.

Compensated polarized light microscopy

Compensated polarized light microscopy (CPLM), which is based on birefringent properties of a material, was used to determine the collagen orientation of samples in this investigation (Cheng et al. 2008). The sample was placed between a polarizer and analyzer, and a full-wave retardation plate is inserted between the sample and the analyzer. The retardation plate (clear gypsum) adds a fixed optical path difference of 530 nm, which enables the identification of the collagen direction through the thickness of the sample (U-TP530; Olympus). Collagen aligned along the slow axis of the retardation plate appears blue and random fiber orientation appears magenta, and the collagen fibers appear in yellow when they are oriented perpendicular to the slow axis (Cheng et al. 2008). A full depth cartilage slice approximately 100 μm thick was sectioned using a razor blade. Images were taken using an upright optical microscope (BX51; Olympus). Samples were placed with the superficial zone oriented 45° to the cross polarizer using a graded rotating sample stage.

Results

Shear displacement caused the initially straight photobleached lines to deform into a sigmoid shape (Fig. 2A1,B1)

(Motavalli et al. 2013). Typically, shear force relaxed in about 2–10 min, with higher strain requiring a longer time to relax (Chung et al. 2012).

Bright fields in polarized microscopy images (Fig. 3A1,A2) showed that the collagen fibers are uniformly parallel to the articular surface in the superficial zone or perpendicular to the articular surface in the radial zone of group A samples. The dark zone showed the randomly oriented collagen fibers belonging to the transitional zone. Furthermore, collagen orientation was inferred by the color scheme in CPLM images (Fig. 3A2). In these samples, collagen fibers in the superficial zone appeared blue, showing the collagen aligned parallel to the articular surface, whereas in the radial zone the collagen fibers are perpendicular to the superficial surface and appear yellow. Between these regions, the transitional zone appeared in magenta and is located at ~10% of full thickness below the surface of group A samples (Fig. 3A1,A2).

Collagen structure in group B (Fig. 3B1,B2) samples was found to be very different from that in group A. In group B samples, polarized light images showed two dark regions instead of one, and CPLM images (Fig. 3B2) showed that the collagen orientations were more random than those in as seen in group A. However, a randomly oriented band of collagen, located between superficial and radial zone, was observed in all group B samples (Fig. 3B1,B2).

For all group A samples, at all increments of shear displacement, the lowest shear strain was found below the articular surface within a band that was 5–15% of the thickness of the sample and the highest strain was found in a

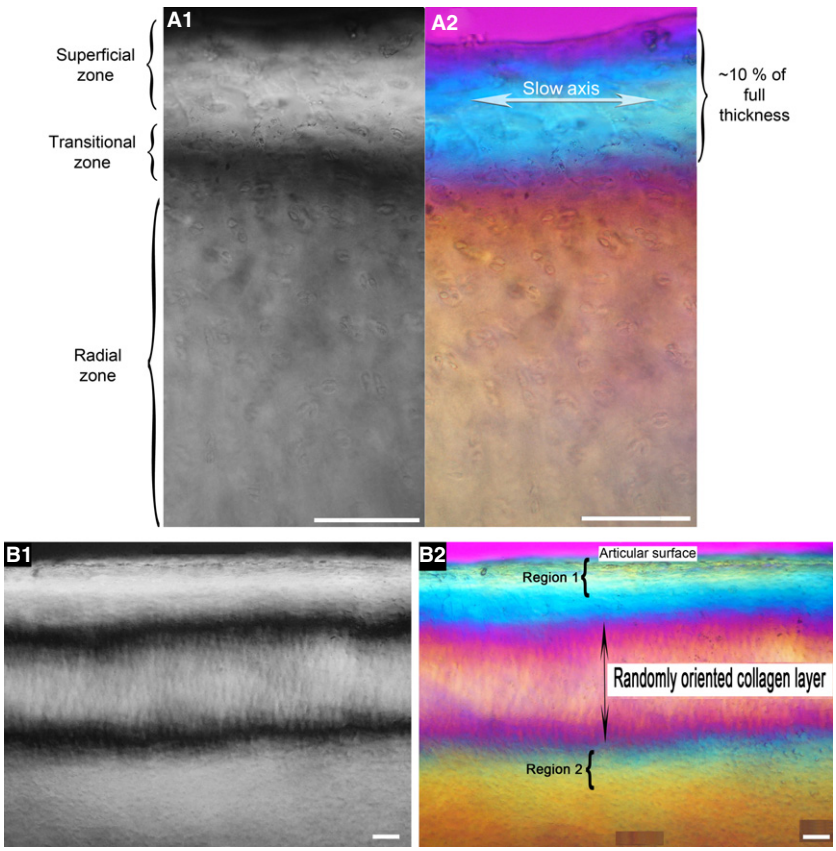

Fig. 3 (A1) Polarized light microscope image of a group A sample shows that collagen fibrils in the superficial and radial zones are aligned either parallel or perpendicular to the articular surface. The dark band in the image shows that there is a region where the fibrils are neither parallel nor perpendicular to the articular surface, which is representative of the transitional zone. (A2) The CPLM image. In the blue region, fibrils are aligned parallel to the articular surface (parallel with the direction of the slow axis of the gypsum plate, arrow), whereas in the yellow region, fibrils are aligned perpendicular to the slow axis. The location of the magenta region corresponds to that of the dark band in the polarized light image where the fibrils are randomly oriented. (B1) Polarized light microscope image from a group B sample shows that there are two regions (dark bands) where the fibrils are neither parallel nor perpendicular to the articular surface. (B2) In the CPLM image, intensely magenta regions correspond to the locations of the transitional regions (dark areas) in the polarized light image. In these regions, fibrils are randomly oriented. The CPLM image further suggests that between the two transitional regions, the orientation of the collagen fibers is a combination of random, perpendicular and parallel to the articular surface. Furthermore, there is yellow region in the superficial zone suggesting collagen fibers perpendicular to the superficial surface. In regions one and two, there are no transitional regions (magenta) in the boundaries between yellow and blue zones, implying lack of smooth transition between the collagen fibers in these regions. Articular surfaces are at the top side of images. Scale bars: 100 μm.

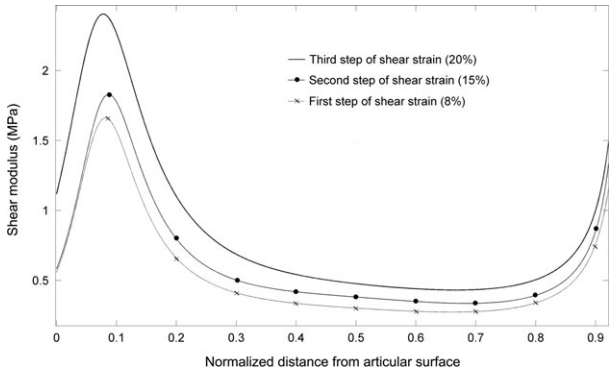

Fig. 4 Full thickness shear modulus profile for three increments of shear strain (8, 15 and 20% average shear strains) (group A). Increasing shear modulus with increasing strain, demonstrates shear-stiffening behavior. Articular surface is at the left side of the picture.

wide band through the radial zone of the sample (Fig. 2A2). It follows that the highest shear modulus was located close to superficial zone and the most compliant region was in radial region (Figs 2A3 and 4). In general, the shear modulus in the region close to the superficial zone was three to four times greater than that in the radial zone (Table 1). It appeared that the location of the stiffest region corresponded with that of the transitional zone (dark region and magenta region in Fig. 3A1,A2). Shear modulus through the mid- to deeper regions was relatively constant before rising again in the deepest part of the radial zone. Additionally, the shear modulus followed the same pattern at all applied shear strains (Fig. 4).

Depth-dependent shear deflection in group B samples was noticeably different from that in group A. In contrast to group A, the maximum shear strain occurred in the superficial zone and it reduced continuously through the radial zone for all group B samples (Fig. 2B2). This showed that the most compliant region in shear was located in the superficial zone, whereas in group A it was in the radial zone. The maximum shear strains in group B were at most seven times larger than those in group A for the same range of mean shear strain. Moreover, notable changes of the shear strain pattern were observed on the borders of the randomly oriented band (Figs 2B2 and 3B2). Break points on the depth-dependent shear strain were observed on the borders of this layer (Fig. 2B2). Moreover, calculated average shear modulus showed that group B samples were stiffer than the group A samples under same shear deflections (Table 1). We also observed that the minimum shear modulus, located in the superficial layer of group B samples (Fig. 2B3), was about five times smaller than the average shear modulus in each shear deflection step.

Samples became stiffer in shear as the strain increased (Figs 4 and 5). Statistical analyses showed that both strain and sample were significant, indicating that overall differences exist between strains and that there is a strong sample effect. Differences in stiffness between the first and second shear strain steps were not significantly different, whereas significant changes in stiffness were found between the first and third, and the second and third steps.

Discussion

The depth-dependent behavior of articular cartilage under simple shear was measured and related to structural organization. Compression was not applied to the sample as it was in previous works (Buckley et al. 2008, 2010, 2013; Canal et al. 2008). We were able to apply shear to the samples since they were bonded to the test apparatus and did not require compression to generate a friction force to transmit shear to the sample. Therefore, the effects of collagen structure on depth-dependent shear behavior without involving compressional effects could be distinguished. Measurements were made in a region of uniform shear stress that best approximates pure shear for this experimental configuration (Chung et al. 2012; Motavalli et al. 2013). Although samples from groups A and B were from the same anatomical location and age range, their depth-dependent shear behavior and collagen structure were found to be very different. There are, of course, some challenges to performing these measurements. Although cartilage is placed between parallel arms of the device, the tissue itself does not necessarily have parallel surfaces. Therefore, sample preparation and securing the samples using adhesives can be a challenging process. Having a flat free imaging surface for the samples is one of the biggest

Table 1 Average measured shear modulus (MPa) ± SD of samples in every incremental shear strain step.

Shear strain steps	1st	2nd	3rd
Average shear modulus (group A)	0.37 ± 0.05	0.44 ± 0.09	0.54 ± 0.13
(minimum; maximum)	(0.32; 0.43)	(0.35; 0.53)	(0.41; 0.69)
Transitional zone maximum shear modulus (group A)	1.00 ± 0.67	1.10 ± 0.75	1.40 ± 0.86
Radial zone minimum shear modulus (group A)	0.23 ± 0.07	0.26 ± 0.07	0.34 ± 0.08
Average shear modulus (group B)	1.20 ± 0.51	1.24 ± 0.54	1.35 ± 0.63
(minimum; maximum)	(0.87; 1.96)	(0.89; 2.05)	(0.91; 2.29)
Superficial zone minimum shear modulus (group B)	0.26 ± 0.12	0.27 ± 0.12	0.29 ± 0.13

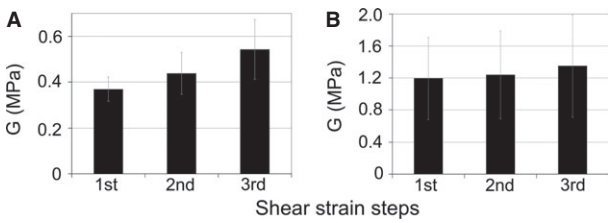

Fig. 5 Average shear modulus of (A) group A and (B) group B samples in three shear strain steps showing that all samples became stiffer as the shear strain increased.

challenges in sample preparation since this free surface is not flattened when using an upright microscope. Unevenness of the surface could affect the sharpness of the image and its uniformity through the entire thickness of the sample (Motavalli et al. 2011, 2012). Glue detachment is another issue that sometimes occurs during the experiment, which affects the shear force profile.

All group A samples had a narrow superficial region (~100 μm) with fibers parallel to the articular surface and a thicker radial zone with fibers perpendicular to the surface (Shahgaldi, 1998; Hunziker et al. 2002, 2007; Canal et al. 2008). Although the superficial zone in group B samples contained fibers that were parallel to the surface, as in group A, this region differed from group A in that it also contained fibers that were radial (Fig. 3B2). The superficial zone in group B samples was about twice as thick as that in group A. A transitional zone, in group A, contained fibers that were neither parallel nor perpendicular to the articular surface, separating the superficial and radial regions. In contrast, below the superficial zone, group B samples had a relatively wide region (~400 μm) with a mix of fiber orientations that was not present in group A samples. The varied orientation of fibers in this region suggests that it might be relatively isotropic compared with the superficial or radial zones. In group A, the radial zone contained fibers that were perpendicular to the surface. Although in group B the radial zone also contained fibers that were perpendicular to the surface, the top of this region was bounded by a layer with fibers that were parallel to the surface (below the randomly oriented layer, Fig. 3B2). These results should be viewed within the limitations of the CPLM method. In these images, the color is blue, magenta or yellow but there is no gradation of these colors. Therefore, we cannot state quantitatively *how* parallel or perpendicular the fiber orientation is, compared with the articular surface.

Structural differences between groups A and B may be due to the skeletal maturity of the animals. It is generally accepted that skeletal maturity (in bovines) occurs between 18 and 24 months of age, which is the range for the animals in this investigation (Kilborn et al. 2002). Structural differences between groups A and B may be due to reorganization of the collagen architecture during the postnatal period, from isotropic in the neonatal period to highly anisotropic when fully matured (Guilak, 1995; Hunziker et al. 2002, 2007; Canal et al. 2008). Although the structure of the samples from group A is indicative of that for mature tissue, the structure in group B, which includes regions with random fiber orientation, suggests that they could still be in the process of maturation (Kim et al. 1995; Kilborn et al. 2002). Staining and acoustic imaging of immature porcine articular cartilage revealed a layer in a location similar to the ones we observed (Kim et al. 1995), which suggests that the group B animal was in the process of maturation. Although samples were harvested from two animals, there were clear differences in structure and shear mechanical behavior. The implications of these structural differences in relation to maturity and mechanical function will be the subject of future studies.

Other mechanical measurements on mature and immature articular cartilage support these observations (Neu et al. 2005; Buckley et al. 2008, 2010; Canal et al. 2008). Using digital image correlation, under conditions resembling joint contact, Canal et al. showed that the radial region undergoes the most shear strain in mature articular cartilage (group A), whereas in immature articular cartilage (group B) the highest shear strain was observed in the superficial zone (Canal et al. 2008). However, direct quantitative depth-dependent shear stiffness comparisons are not possible since the shear stress distribution in Canal et al., was not determined. Our results are consistent with those of Buckley et al. for neonatal bovine AC. Both cases showed an overall decrease in shear strain with increasing depth (Fig. 2B2). However, loading conditions are not directly comparable: Buckley et al. (2008, 2010) used oscillating shear deflections with a constant compressive load, whereas our measurements were made under static conditions without compression. Moreover, the age differences of the animals studied in this and other investigations may give rise

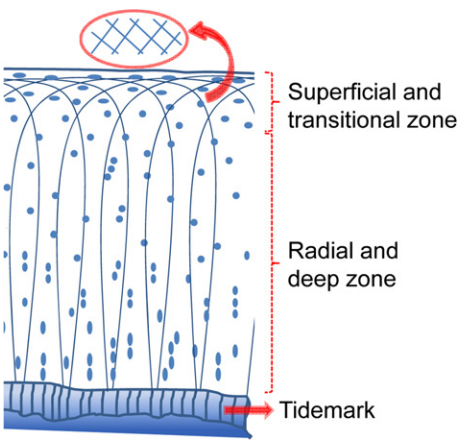

Fig. 6 A schematic for mature articular cartilage shows the structured collagen architecture and anisotropic morphology. Long slender fibers in the radial zone are expected to provide little resistance to shear. In contrast, the crossed fibers in the transitional region could provide a structure that is stiff in shear, consistent with the results we have found for mature articular cartilage.

to this small variation of shear deflection close to the superficial zone.

Comparing collagen structure and shear strain between groups A and B suggests significant effects of microstructure in depth-dependent shear mechanical behavior. As collagen structure of group B samples differed from group A, the shear strain patterns changed as well as the location of the most compliant regions (Figs 2 and 3). Variations in the depth-dependent structure of group A samples suggested a model for the computed variations in shear stiffness through the depth of the tissue (Figs 3A1, 3A2 and 6). Results showed that the location of the transitional zone corresponded with the minimum shear strain (shear modulus peak). Crossed fibers in the transitional region could be providing a structure that is stiff in shear, similar to diagonal braces in a simple rectangular frame. In contrast, low stiffness in the radial zone could be due to minimal cross bracing of these fibers, which would then have little resistance to shear applied perpendicular to their length (Fig. 6). In addition to the structure, morphological and histological properties of collagen fibers such as length, thickness and their connectivity may affect the depth-dependent mechanical behavior. On the other hand, group B samples showed a more complex pattern of collagen structure than group A, which is reflected in different depth-dependent shear behavior. In group A, there is a transitional zone (magenta) between superficial (blue) and radial (yellow) zones that smoothly transforms the collagen fiber orientations from vertical in the radial zone, to horizontal in the superficial zone. In contrast, there are no transitional regions (magenta) in the boundaries between yellow and blue zones in regions one and two in group B (Fig. 3B2). This may suggest that the collagen directions do not smoothly transform between these two regions and hence these layers may not be as structurally integrated in group B as they may be in group A. This may give cause higher shear strain on the layers close to the superficial surface than on the radial layer in group B. However, compensated polarized light microscopy had limitations in detecting these histological properties, which restricted our ability to find a definitive model explaining collagen structure and depth-dependent shear behavior relationship.

In summary, the shear properties of bovine articular cartilage were determined without applied compression. These results appeared to be feasible based on structural arguments. Comparison of results also suggests that in addition to species and anatomic location, age needs to be considered when reporting such results where macromolecular structures play an important role in mechanical properties of the tissue.

Acknowledgements

This work was funded by the National Institutes of Health (Grant number P01 AR053622). The content is solely the responsibility of the authors and does not necessarily represent the official views of the National Institutes of Health. The authors would like to thank Dr. Mark Schluchter for his advice and assistance with the statistical analysis used in this work.

Contributors

All authors worked collectively to develop the protocols and methods described in this paper. They all contributed to the analysis and interpretation of the results. J.M.M. was the principal investigator responsible for overall direction of the work, and M.M. conducted experiments and image-processing. O.A. contributed the expertise for the compensated polarized light microscopy studies. M.M. and J.M.M. wrote the report. All authors read, modified and approved the final report.

Conflict of interest

The investigators have no conflict of interest to declare.

Role of the funding source

The study sponsors played no role in the study design, the collection, analysis, and interpretation of data, writing of the report, or the decision to submit the paper for publication. The corresponding author had full access to all the data and had the final decision to submit for publication.

References

Athanasiou KA, Rosenwasser MP, Buckwalter JA, et al. (1991) Interspecies comparisons of in situ intrinsic mechanical properties of distal femoral cartilage. *J Orthop Res* **9**, 330–340.

Bruehlmann SB, Matyas JR, Duncan NA (2004) Collagen fibril sliding governs cell mechanics in the anulus fibrosus. *J Spine* **29**, 2612–2620.

Buckley MR, Gleghorn JP, Bonassar LJ, et al. (2008) Mapping the depth-dependence of shear properties in articular cartilage. *J Biomech* **41**, 2430–2437.

Buckley MR, Bergou AJ, Fouchard J, et al. (2010) High-resolution spatial mapping of shear properties in cartilage. *J Biomech* **43**, 796–800.

Buckley MR, Bonassar LJ, Cohen I (2013) Localization of viscous behavior and shear energy dissipation in articular cartilage under dynamic shear loading. *J Biomech Eng* **135**, 0310021–0310029.

Canal CE, Hung CT, Ateshian GA (2008) Two-dimensional strain fields on the cross-section of the bovine humeral head under contact loading. *J Biomech* **41**, 3145–3151.

Cheng X, Gurkan UA, Dehen CJ, et al. (2008) An electrochemical process for assembly of anisotropically oriented collagen bundles. *Biomaterials* **29**, 3278–3288.

Chung C, Motavalli M, Mansour JM (2012) Stress relaxation of cartilage under simple shear and compression: experiments and finite element analyses. In: ASME Summer Bioengineering, Puerto Rico. ASME,

Guilak F (1995) Compression-induced changes in the shape and volume of the chondrocyte nucleus. *J Biomech* **28**, 1529–1541.

Hosoda N, Sakai N, Sawae Y, et al. (2008) Depth-dependence and time-dependence in mechanical behaviors of articular cartilage in unconfined compression test under constant total deformation. *J Biomech Sci Eng* **3**, 209–220.

Hunziker EB, Quinn TM, Hauselmann HJ (2002) Quantitative structural organization of normal adult human articular cartilage. *Osteoarthritis Cartilage* **10**, 564–572.

Hunziker EB, Kapfinger E, Geiss J (2007) The structural architecture of adult mammalian articular cartilage evolves by a synchronized process of tissue resorption and neoformation during postnatal development. *Osteoarthritis Cartilage* **15**, 403–413.

Kilborn SH, Trudel G, Uhthoff H (2002) Review of growth plate closure compared with age at sexual maturity and lifespan in laboratory animals. *Contemp Top Lab Anim Sci* **41** (No.5), 21–26.

Kim HKW, Babyn PS, Harasiewicz KA, et al. (1995) Imaging of immature articular cartilage using ultrasound backscatter microscopy at 50 MHz. *J Orthop Res* **13**, 963–970.

Motavalli M, Whitney GA, Dennis J, et al. (2011) Mansour Mechanical Behavior and Failure of Scaffold Free Tissue Engineered Cartilage. In: Biomedical Engineering Society annual meeting, Hartford, Connecticut.

Motavalli M, Chung C, Schluchter M, et al. (2012) A continuous shear deflection function for articular cartilage. In: ASME Summer Bioengineering, Puerto Rico. ASME,

Motavalli M, Whitney GA, Dennis JE, et al. (2013) Investigating a continuous shear strain function for depth-dependent properties of native and tissue engineering cartilage using pixel-size data. *J Mech Behav Biomed Mater* **28**, 62–70.

Neu CP, Hull ML, Walton JH (2005) Heterogeneous three-dimensional strain fields during unconfined cyclic compression in bovine articular cartilage explants. *J Orthop Res* **23**, 1390–1398.

Schinagl RM, Ting MK, Price JH, et al. (1996) Video microscopy to quantitate the inhomogeneous equilibrium strain within articular cartilage during confined compression. *Ann Biomed Eng* **24**, 500–512.

Shahgaldi BF (1998) Repair of large osteochondral defects: load-bearing and structural properties of osteochondral repair tissue. *Knee* **5**, 111–117.

Wong BL, Sah RL (2010) Mechanical asymmetry during articulation of tibial and femoral cartilages: local and overall compressive and shear deformation and properties. *J Biomech* **43**, 1689–1695.